

Implementation and Comparison of Electron Cloud Measurements at the Cornell Electron Storage Ring

Benjamin Carlson*

Grove City College, PA 16127

Michael Billing, Mark Palmer, and John Sikora

Laboratory of Elementary Particle Physics,

Cornell University, Ithaca, NY 14853

Electron cloud buildup is ubiquitous in positron accelerators, and can lead to unwanted effects including beam degradation. Thus, significant efforts have been directed toward characterizing electron cloud effects by retarding field analyzers (RFA) and TE Wave measurements. While past TE Wave work has used a propagating wave, we have also used an evanescent or resonant mode for determining electron cloud density. This eliminates a number of ambiguous aspects associated with the propagating mode. Furthermore, we have compared the propagating with resonant TE Wave measurements, and RFA data with TE Wave data.

I. INTRODUCTION

The International Linear Collider (ILC) is a proposed e^+e^- collider designed to study phenomena at energies less than 1TeV. ILC damping rings (ILCDR) will be critical in the production of low emittance beams. The high luminosity and simplicity of e^+e^- collisions will allow the ILC to study phenomena with more precision than the Large Hardron Collider (LHC)[1]. It has been proposed that the the ILC may be used to study electroweak symmetry breaking, supersymmetric parti-

cles, and dark matter candidates [2, 3].

The ILCDR and a number of other accelerators, such as the Tevatron Main Injector [4] and the accumulation ring of the Spallation Neutron Source, will operate in a parameter regime affected by low density electrons referred to as the Electron Cloud (EC) [5]. Low energy photoelectrons are emitted from the beam pipe by synchrotron radiation, then are accelerated by the field of the beam. These high energy electrons are then capable of causing secondary electron emission from collisions with the wall of the beam pipe. If the traversal time of the chamber matches the

*Electronic address: carlsonbt1@gcc.edu

bunch spacing, an amplification of the EC occurs which is referred to as multipacting [6].

Though EC effects are ubiquitous in high energy accelerators, multipacting can result in vacuum degradation and other effects detrimental to beam dynamics. For instance, coupled bunch interactions can result in vertical beam instabilities [7] and beam tune shift [8]. In addition, single bunch head-tail effects can result from coherent oscillation along the bunch, and lead to emittance growth [9, 10].

The magnitude of the electron cloud density (ECD) is dependent on factors such as surface geometry, photoelectron characteristics, secondary electron yield (SEY), bunch current and bunch spacing [11, 12]. EC mitigation techniques such as the use of a coating to reduce the SEY, groove geometry, clearing electrodes, and the use of a solenoid field to confine electrons near the beam pipe walls are being investigated [13–15].

Several techniques for directly measuring EC properties have been developed. A Retarding Field Analyzer (RFA) measures local electron flux leaving the beam pipe, and can be related to the ECD, and the use of a retarding grid can allow for energy characterization [16]. In addition, microwave dispersion measurements (TE Wave) have recently been used to measure the ECD over an extended region of beam pipe [17]. Finally, we

have used a novel technique with an evanescent, rather than propagating TE Wave to measure the ECD.

At the Cornell Electron Storage Ring (CESR) both RFA's and TE Wave techniques have been employed to measure EC characteristics in wigglers which will be a major component of the ILCDR. In addition, studies have been done in the adjustable dipole field of a Chicane magnet and drifts. Various mitigation techniques, including surface coatings of TiN on aluminum and copper, as well as solenoid windings are also being investigated.

Due to the complexity of EC phenomena, it is desirable to obtain a comparison between transmission and evanescent TE Wave techniques with each other and RFA data. This will allow for better understanding of EC measurements, and subsequently EC phenomena, such as the effect of magnetic fields, SEY curves as a function of electron energy, and EC lifetime. Such understanding will enable more robust models to be developed and applied to modern accelerators.

II. RFA ELECTRON CLOUD MEASUREMENT

RFA's work on the principal of measuring incident electron flux at the beam pipe wall. As depicted in Fig. 1, the RFA consists of

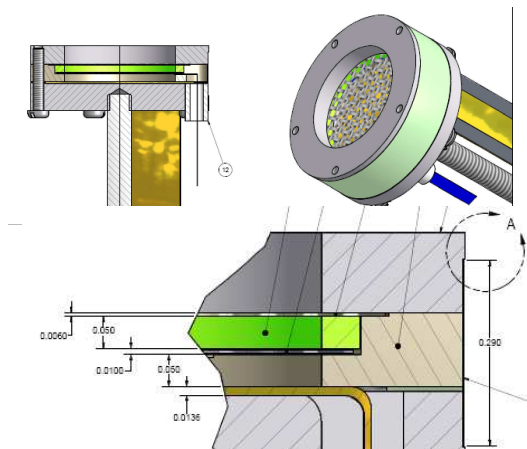


Figure 1: RFA schematic

a retarding grid structure with collector for measuring an electron current, as described in [30]. The calculation of ECD from RFA current data is non-trivial, since RFA's measure an electron flux at the edge of the beam pipe. However, a method has been devised for calculating an ECD by a POSINST simulation for the beam pipe and RFA, which is then compared with measured RFA currents [31]. This method was used to calculate RFA densities, but it is preliminary, and does not include an actual simulation of the RFA, for effects such as secondary electron emission from the RFA grid.

III. MICROWAVE ELECTRON CLOUD MEASUREMENT TECHNIQUES

The EC is often modeled as a plasma, and there are a number of techniques for deter-

mining plasma characteristics, including density. Plasma characterization methods include the use of a probe [18], microwave absorption, reflection, and interferometry [24]¹ are often difficult to implement since the plasma density is low ($10^{12} e^-/m^3$), and the inside of the beam pipe not easily accessible. Thus, it is desirable to develop parasitic techniques for measuring the EC using beam position monitors (BPM). Use of microwave techniques to measure the ECD involve the oscillation of electrons[18], which in a plasma can be shown to have a characteristic frequency dependent only on the density,

$$\omega_p = \sqrt{\frac{e^2 n_e}{m_e \epsilon_0}} \approx 56.4 \sqrt{n_e} \quad (1)$$

where n_e is the ECD in e^-/m^3 , e is the charge of an electron, m_e the mass of an electron, and ϵ_0 the permittivity of free space. This equation was derived for a neutral plasma considering only the effect of the free electrons. In this approximation, the ion mass is much greater than the electron mass, and consequently the ion motion is assumed to be negligible.

A. Transmission method

As depicted in Fig. 2, the EC fluctuates with the beam current, and the modulated

¹ pp 192-228

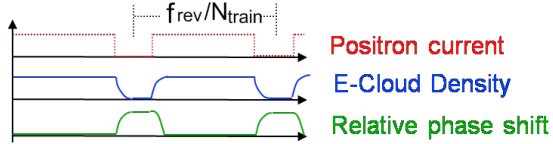


Figure 2: Bunch trains modulate the EC,
which can be detected as a phase
modulation in a propagating TE Wave

microwave signal is modulated by some function $\theta(t)$. Since any periodic oscillation can be represented as a Fourier series, $\theta(t)$ can be written as

$$\theta(t) = \sum_{n=1}^{\infty} [a_n \cos(n\omega_{rev}t) + b_n \sin(n\omega_{rev}t)] \quad (2)$$

where the arbitrary DC offset is neglected and ω_{rev} the angular frequency of modulation. In the case of CESR, the phase is modulated at the revolution frequency of the accelerator, or $f_{rev} = 390\text{KHz}$.

Well above cutoff, a waveguide can support TE Waves, not to be confused with low frequency plasma (TG) waves [19]. The transmission of a TE Wave through a transient plasma allows the density averaged over the direction of propagation to be determined. The index of refraction of the EC causes a phase shift to accumulate in the propagating wave [17]. The dispersion relation in a waveguide filled with a uniform plasma has been derived analytically [21], and been verified using VORPAL code [22].

It is given by the relatively simple expression,

$$k^2 = \frac{\omega^2}{c^2} - \frac{\omega_p^2}{c^2} - \frac{\omega_c^2}{c^2} \quad (3)$$

where k is the wavenumber and ω_c the cut-off frequency of the beam pipe. The phase advance is then given by,

$$\Delta\phi = \frac{L\omega_p^2}{2c\sqrt{\omega^2 - \omega_c^2}} \quad (4)$$

where L is the distance of propagation. As shown by [17, 22], proximity to cutoff has an amplifying affect on $\Delta\phi$, though the total phase shift is typically on the order of milliradians.

The phase modulation can be measured by observing the signal in the frequency domain, which allows for the measurement of small phase shifts that would otherwise be difficult to detect. Letting eq. 2 take the form of $\Delta\phi \cos(\omega_{rev}t)$, where $\Delta\phi$ is the maximal phase shift, an expression for the waveform is,

$$M(t) = A \sum_{n=-\infty}^{\infty} J_n(\Delta\phi) \cos[(\omega - n\omega_{rev})t - \frac{n\pi}{2}] \quad (5)$$

where J_n is a Bessel function of the first kind. The amplitude of the sidebands are given by the coefficients, and the frequency spectrum by discrete multiples of the revolution frequency ω_{rev} . As a result the phase modulation produces sidebands at 390KHz from the carrier frequency, as shown in Fig. 3. The ra-

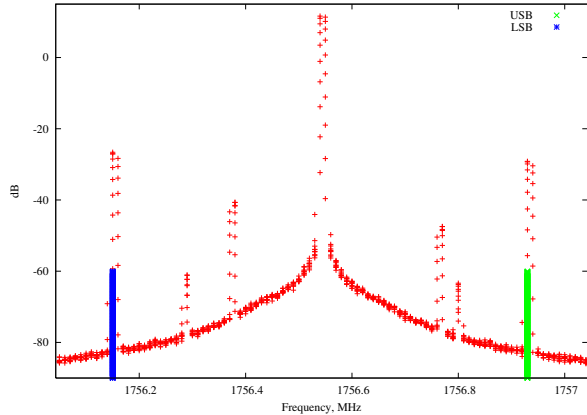


Figure 3: Typical frequency spectrum, with the drive frequency is shown in the center, and the upper and lower sidebands highlighted.

ratio of the first sideband to the carrier is given by

$$\frac{A_{sb}}{A_{car}} = \frac{J_1(\Delta\phi)}{J_0(\Delta\phi)} \approx \frac{\Delta\phi}{2} \quad (6)$$

where all higher order terms of the Bessel functions were truncated, which is valid for small $\Delta\phi$. Combining eq. 4 with eq. 1 and eq. 6 gives the ECD as a function of sideband amplitudes.

$$n_e = \left(\frac{8\pi m_e \varepsilon_o}{e^2} \right) \left[\frac{A_{sb}}{A_{car}} \right] \frac{c\sqrt{f^2 - f_c^2}}{L} \quad (7)$$

B. Resonant method

It is well known that driving a waveguide below cutoff produces a so-called evanescent wave, as approximately depicted by Fig. 4. Such a mode is non-propagating, as shown

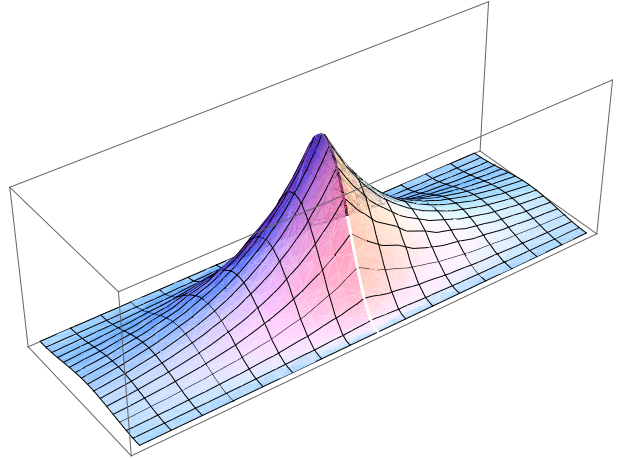


Figure 4: The approximate distribution of the y component of the electric field, where the drive point is near the maximum, and decays exponentially in the longitudinal direction.

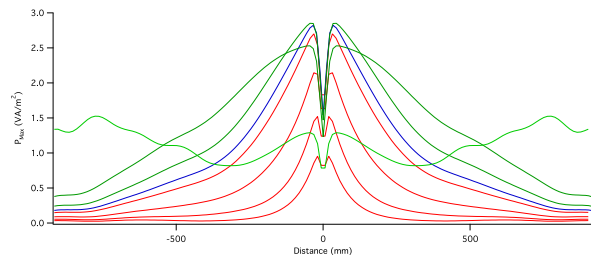


Figure 5: [S. De Santis] Magnitude of the Poynting vector vs. Distance from BPM. Red curves represent drive frequencies below cutoff, blue at cutoff, and green above cutoff. The simulation was performed in Microwave Studio, using the the dimensions for the beam pipe in L0.

by red curves in Fig. 5. The waveguide was driven at the resonance of the evanescent mode, so assuming perfectly conducting

walls, only one mode was excited [26]².

The presence of a plasma perturbs the resonant frequency and the Q of the mode [24, 27, 29]. The perturbing electron plasma can be treated as a complex dielectric, given by

$$\varepsilon = \varepsilon_o \left[1 - \frac{\omega_p^2}{\omega(\omega - i\nu)} \right] \quad (8)$$

where $i = \sqrt{-1}$ and ν is the angular collision frequency, where the real part, $\varepsilon_r = \text{Re}[\varepsilon]$, effects the frequency shift and is given by,

$$\varepsilon_r = \varepsilon_o \left[1 - \frac{\omega_p^2}{\omega^2(1 + \gamma^2)} \right] \quad (9)$$

where $\gamma = \frac{\nu}{\omega}$. The frequency shift due to the presence of the dielectric can be found using perturbation theory, and is then given by [27]

$$\frac{\Delta f}{f} = - \frac{\int_{V'} (\varepsilon_r - \varepsilon_o) |E_y|^2 dV'}{4U_o} \quad (10)$$

where U_o is the stored energy of the cavity, and $|E_y|$ the magnitude of maximum field in the cavity. Since the energy oscillates between the electric and magnetic fields, the energy in the maximum magnetic and electric fields are equal. Similarly, the stored energy is given by [25]³,

$$U_o = \int_V \frac{\varepsilon_r}{2} |E_y|^2 dV \quad (11)$$

Also assuming a uniform plasma, which completely fills the cavity ($V'=V$), eq. 10 drastically simplifies, yielding,

$$\frac{\Delta f}{f} = \frac{1}{2} \left[\frac{\frac{f_p^2}{f^2(1+\gamma^2)}}{1 - \frac{f_p^2}{f^2(1+\gamma^2)}} \right] \quad (12)$$

In principle it is possible to measure the resonant frequency shift directly, however, this experiment was not performed. Equation 2 can be written as $-\Delta\omega_c \sin(\omega_{rev}t)$, where $\Delta\omega$ is the maximum angular frequency modulation over a turn. Assuming a frequency modulating function of yields a waveform $M(t)$,

$$M(t) = A \sum_{n=-\infty}^{\infty} J_n\left(\frac{\Delta\omega_c}{\omega_{rev}}\right) \cos\left[(\omega_c + n\omega_{rev})t + \frac{n\pi}{2}\right] \quad (13)$$

The ratio of the first sideband amplitude to the carrier amplitude can then be written as,

$$\frac{A_{sb}}{A_{car}} = \frac{J_1\left(\frac{\Delta\omega_c}{\omega_{rev}}\right)}{J_0\left(\frac{\Delta\omega_c}{\omega_{rev}}\right)} \approx \frac{1}{2} \frac{\Delta\omega_c}{\omega_{rev}} = \frac{1}{2} \frac{\Delta f_c}{f_{rev}} \quad (14)$$

Typical spectra yield a ratio of sidebands much less than one, so the approximation is valid.

Re-arranging then substituting eq. 14 and eq. 1 into eq. 12 yields

$$n_e = \left(\frac{4\pi^2 m_e \varepsilon_o}{e^2} \right) \left[\frac{A_{sb}}{A_{car}} \right] \frac{4f f_{rev} (1 + \gamma^2)}{\left[\frac{A_{sb}}{A_{car}} \right] \frac{4f_{rev}}{f} + 1} \quad (15)$$

² 534-539

³ pp. 543

For $\nu \ll \omega$, which is valid for a low density collisionless plasma, eq. 15 becomes,

$$n_e = \left(\frac{4\pi^2 m_e \varepsilon_o}{e^2} \right) \left[\frac{A_{sb}}{A_{car}} \right] \frac{4f f_{rev}}{\left[\frac{A_{sb}}{A_{car}} \right] \frac{4f_{rev}}{f} + 1} \quad (16)$$

Note that the denominator is approximately equal to unity for typical parameters, and as a result, the effect of the cloud density on the stored energy for a uniform density is negligible. A number of limitations concerning the use of a microwave cavity to measure electron density have been brought up [29]. In particular, upper and lower limits on the density of plasma detectable have been calculated. However, assuming a collisionless plasma, the bounds on the measurement will primarily be determined by experimental limitations rather than theoretical limits. For a dynamic range of 70dB, this gives a range in densities measurable from 10^{10} to $3 \times 10^{13} e^-/m^3$, assuming the upper bound is given when the intensity of the sideband equals the intensity of the carrier.

Up to this point - no assumption regarding beam pipe geometry has been made. However - if we assume a rectangular beam pipe of width a , the effect of a non-uniform plasma in eq. 10 is not difficult to calculate. For instance, a plasma concentrated in the center of the beam pipe with extent 2ζ in x , and uniform in y , can be described by a piecewise

function, with density n_o

$$n(x, y) = \begin{cases} 0 & 0 < x < \frac{a}{2} - \zeta \\ n_o & \frac{a}{2} - \zeta < x < \frac{a}{2} + \zeta \\ 0 & \frac{a}{2} + \zeta < x < a \end{cases} \quad (17)$$

If we re-write eqn's. 10, 11, and 14 assuming that the stored energy is close to that with $\varepsilon_r = \varepsilon_o$, and the plasma is collisionless, we find the density n_o .

$$n_o = \left(\frac{8\pi^2 m_e \varepsilon_o}{e^2} \right) \left[\frac{A_{sb}}{A_{car}} \right] \frac{f_{rev} f a}{\int_{\frac{a}{2}-\zeta}^{\frac{a}{2}+\zeta} \sin^2 \left(\frac{\pi x}{a} \right) dx} \quad (18)$$

Note that the integral goes to 0 outside of the plasma, and that the field in the TE_{01} mode is given by $|E_y|^2 = E_o^2 \sin^2 \left(\frac{\pi x}{a} \right)$.

C. Correction for Modulation Shape

We have assumed that the modulation is a sine or cosine function. Since the production of the EC follows the passage of the bunch train, the peak ECD must be corrected. Given a modulating function

$$f(t) = \begin{cases} 0 & -\frac{T}{2} < t < -t_1 \\ 1 & -t_1 < t < t_1 \\ 0 & t_1 < t < \frac{T}{2} \end{cases} \quad (19)$$

where $2t_1$ is the duration of the pulse, and T the period, the function $f(t)$ can then be written as a Fourier series,

$$f(t) = a_o + \sum_{n=1}^{\infty} (a_n \sin(n\omega t) + b_n \cos(n\omega t)) \quad (20)$$

The components can be found from the following integrals,

$$a_n = \frac{2}{T} \int_{-\frac{T}{2}}^{\frac{T}{2}} f(t) \sin(n\omega t) dt \quad (21)$$

$$b_n = \frac{2}{T} \int_{-\frac{T}{2}}^{\frac{T}{2}} f(t) \cos(n\omega t) dt \quad (22)$$

Since $f(t)$ is symmetric about the origin, the a_n 's are all 0, and we can simply evaluate eq. 22 for the function given by eq. 19, which yields,

$$b_n = \frac{2}{n\pi} \sin\left(\frac{2n\pi t_1}{T}\right) \quad (23)$$

Since only the first term in the series was measured, we only need be concerned with b_1 , and can correct eq. 7 and eq. 16 by dividing by b_1 . Assuming a 45 bunch 4ns train, and a revolution period of $2.5\mu S$, this yields to a correction factor of $b_1 = 0.14$. This suggests that the the instantaneous density is greater by a factor of about 10.

Sensitivity Comparison

Taking eq. 7 and eq. 15, and solving for the ratio of sideband amplitudes as a function of density yields,

$$\varphi \equiv \frac{c}{4\pi} \left[\frac{\sqrt{f^2 - f_c^2}}{f_{rev} f L \left(1 - \frac{n_e}{\alpha f^2}\right)} \right] \quad (24)$$

where $\alpha = \frac{4\pi^2 m_e \epsilon_o}{e^2}$. Using the L0 parameters for f and f_c shown in Table I, and a value of $n_e = 10^{12}$, the ratio is equal to unity when $L=8.5m$. Thus a similar sensitivity between the methods with the transmission measurement is acquired over approximately 10m. In a similar manner, it can be argued that the evanescent mode is almost an order of magnitude more sensitive to local cloud density, assuming the field extends one meter in the longitudinal direction (see Fig. 5).

IV. EXPERIMENTAL SETUP

The lowest TE mode was used for all experiments. In the L0 region, the beam pipe is approximately rectangular, as depicted in Fig. 6, so the electric field has a maximum in the center of the pipe - and is zero at the boundaries. Thus, it can be argued that the TE Wave method is most sensitive to the EC in the center of the pipe. The pipe geometry in the L3 region is circular, which means that the fields vary as $J_o(kr)$ instead of $\sin\left(\frac{\pi x}{a}\right)$, which is still peaked at the center of the beam pipe.

The driving frequency was chosen to be above cutoff for the first mode, well below cutoff for higher order modes, near a local

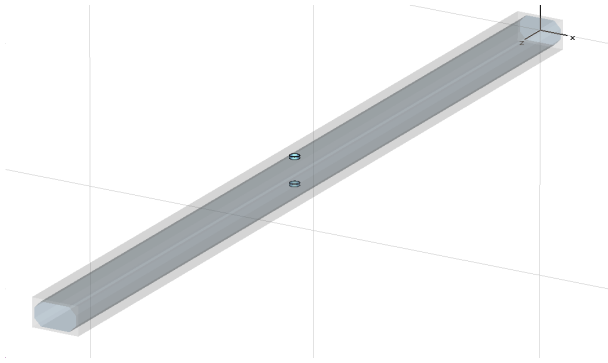


Figure 6: L0 Beam pipe geometry

peak, and away from revolution harmonics. In practice ω_c was difficult to determine because the transfer function of the beam pipe did not have a smooth well defined transition to a propagating wave. The evanescent mode is by definition non-propagating, so it was assumed that the resonant frequency for the evanescent mode must be close to the cut-off frequency of the propagating mode.

A set of diagnostic experiments were performed to examine transmission of the TE_{01} mode in the beam pipe. In the L3 region, the amplitude of the transmitted signal was measured at BPMs extending 30-40 meters in each direction. It was found that the signal rapidly attenuated after the 48E and 48W BPMs, which were used for the May-June machine studies.

Since the beam pipe has discontinuities and changes in geometry, it was desirable to look for pulse reflections in the beam pipe. As shown in Fig. 7, 49→48E transmission at 2.06517GHz when driven with a 1 μ s pulse

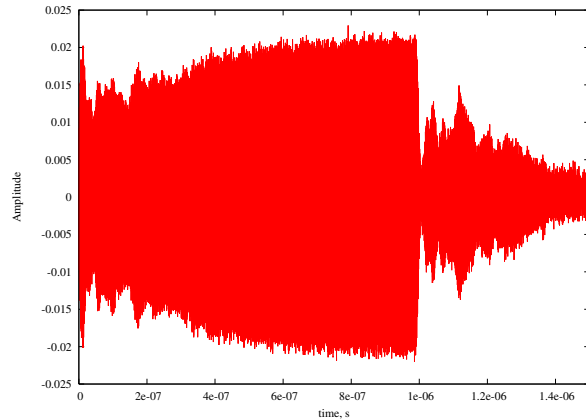


Figure 7: Response of 49 to 48E at 2.06517GHz to a 1 μ s pulse

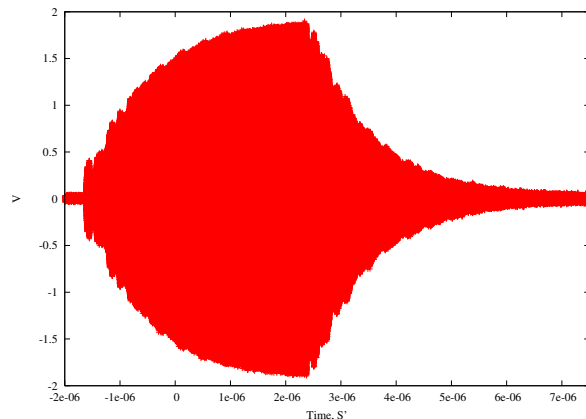


Figure 8: Sample response to a 2 μ s pulse of the 0W resonant detector at 1.77892GHz

showed a fairly rapid decay after the end of the pulse, opposed to a resonant mode, where the characteristic decay is more gradual, as depicted in Fig. 8. However, a pulse driven at a frequency of 2.02224GHz from 49→48W shows a smooth decay after the end of the driving pulse (data not shown). The transfer function shown in Fig. 9 has a number of peaks above cutoff, which suggests that reflections may become important in the prop-

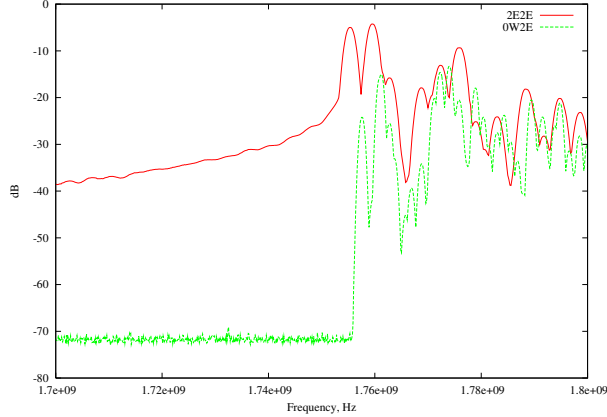


Figure 9: Transfer function for a resonant cavity mode (0E0E) and for a transmission mode (0W2E)

agating mode.

Since the sideband and carrier frequencies are not identical, the frequency response at the sideband location may differ from the carrier depending on the frequency response. An attempt to correct for this systematic error was made by carefully measuring the transfer function on a 1MHz span, as shown in Fig. 10. However, this experiment also revealed that the peaks have a tendency to drift, which can be explained by thermal contraction and expansion of the beam pipe.

The May-June experimental period recorded data in both the L3 and L0 experimental regions, using the setup shown in Fig. 11. A drive signal, produced using Agilent Technologies, N5181A 100KHz-6GHz signal generator was in conjunction with a 5W amplifier to transmit RF into the beam pipe through an opposing set of BPMs, as

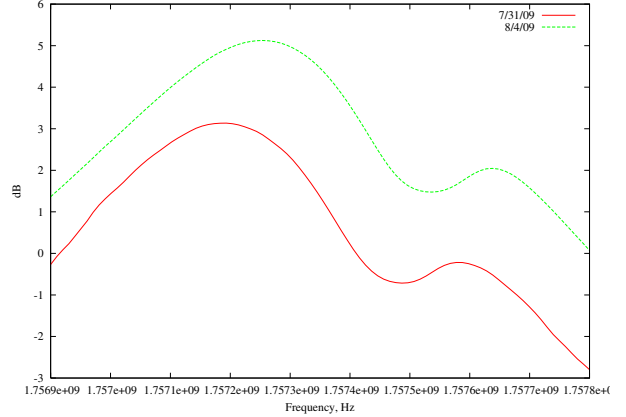


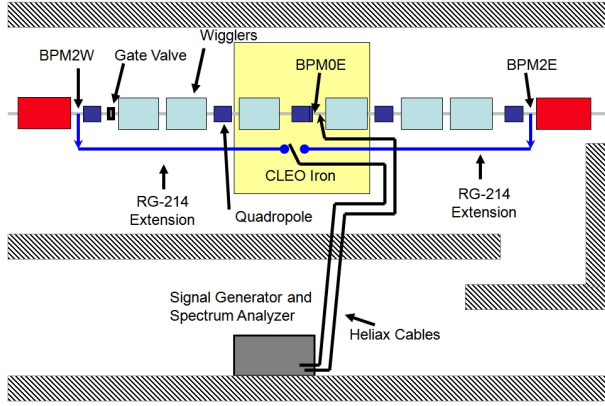
Figure 10: The local transfer function for the 0E0E detector, measured on two different days showing a peak shift

shown in Fig. 12. Agilent Technologies N9020A 20Hz-26.5GHz spectrum analyzer was used to measure modulated RF. All time domain studies were performed using a Lecroy WaveMaster 804Z 4GHz Oscilloscope. Experimental parameters are given in Table I; lengths were determined from the CESR lattice file.

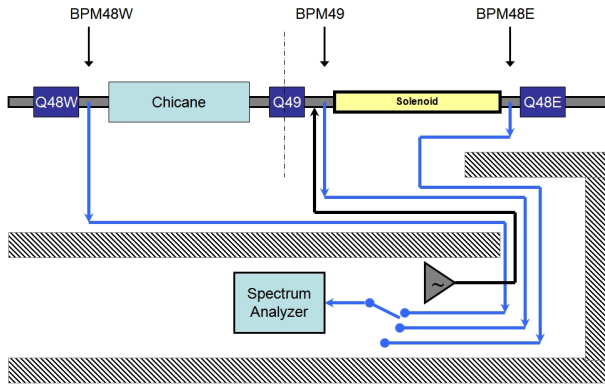
Data was recorded at 2.085 and 5GeV, however the signal-to-noise ratio at 2.085GeV was generally low. Thus, all data shown in this paper will be at 5GeV, unless specifically noted. For two peaks, 1 and 2 given in units of dB in the frequency spectrum, the ratio of amplitudes is given by,

$$\Delta dB = dB_2 - dB_1 \quad (25)$$

$$\frac{A_2}{A_1} = 10^{\Delta dB/20} \quad (26)$$



(a) L0 setup



(b) L3 setup

Figure 11: Experimental setup for L0 (11a) and L3 (11b)

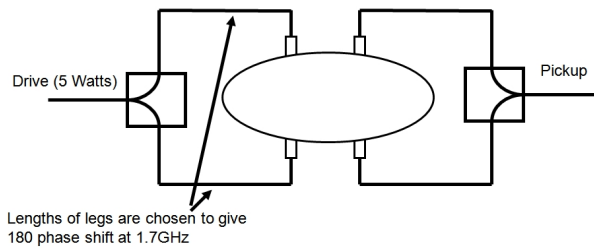


Figure 12: Drive / Pickup configuration using BPM

Location	Drive Frequency, GHz	Length (L), m
49 → 49	1.95242	-
49 → 48E	2.06517	3.93
49 → 48W	2.02224	5.70
0E → 0E	1.756543	-
0E → 2E	1.8275775	8.29
0E → 2W	1.8275775	9.09

Table I: Experimental parameters for May-June data run

Location	Drive Frequency, GHz	Length (L), m
49 → 49	1.95242	-
49 → 48E	2.06517	3.93
49 → 48W	2.02224	5.70
0W → 0W	1.75738	-
2E → 2E	1.7554	-
2W → 2W	1.7601	-
0W → 2E	1.76126	7.46
0W → 2W	1.81823	8.3

Table II: Experimental parameters for July-August data run

V. RESULTS

The rectangular geometry of the beam pipe in the wiggler region, and increased

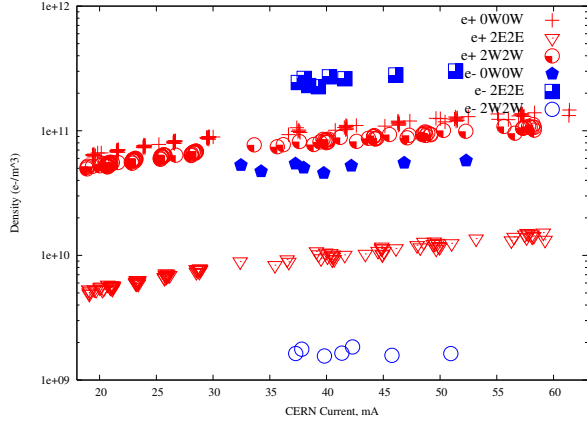


Figure 13: Comparison of electrons and positrons from resonant detectors, with wigglers on at 2GeV from the July-August data run, bunch pattern 8x5. The data was plotted on a log y scale.

signal-to-noise made this region an ideal place to begin analysis. As depicted in Fig. 13, the resonant detectors with wigglers on suggest that greater light is down stream of the beam direction. For instance, for electrons, the greater signal is seen in the East, while for positrons the signal is much greater in the West.

The profile of the synchrotron light is not uniform, as shown in Fig. 14 and can be detected by TE Wave measurements.

Transmission and resonant TE Wave measurements were compared for a consistency check with each other and RFA measurements. When the modulating function is assumed to be a cosine function, then the TE Wave measures the average ECD, which is

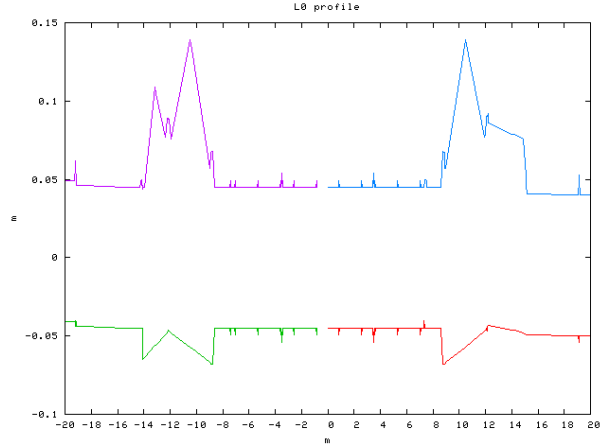


Figure 14: Profile of Synchrotron radiation in the L0 wiggler region

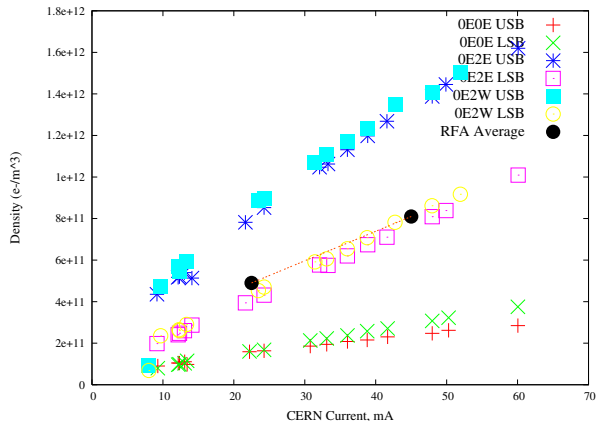


Figure 15: Average density measurements with wigglers on, comparing resonant and transmission measurements with RFA data.

May-June data at 5GeV, 45 bunch train, 4ns spacing. No correction was made for the modulation shape.

depicted in Fig. 15. The peak density was calculated assuming a square pulse modulation, and is depicted in Fig. 16. Along the same lines, since the peak density is easy to calculate from eq. 23, a study was done of

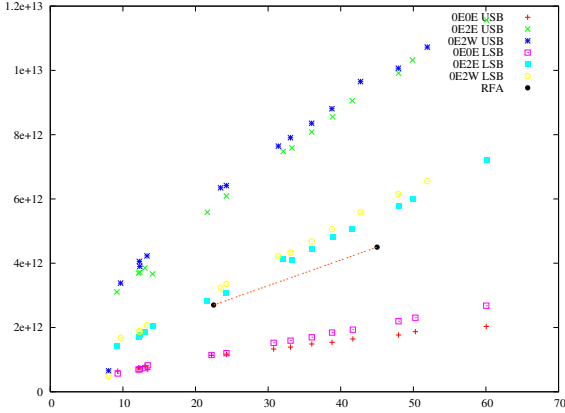


Figure 16: Peak density measurements with wigglers on, comparing resonant and transmission measurements with RFA data. May-June data at 5GeV, 45 bunch train, 4ns spacing.

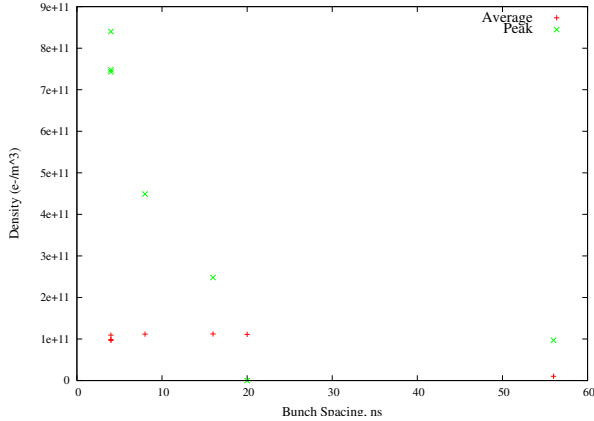


Figure 17: Average and peak densities at the resonant detector, 5GeV, wigglers on from the May-June data run.

the ECD as a function of bunch spacing, as depicted in Fig. 17.

Studies in the Chicane region, with the field of the chicane off show in Fig. 18 that the resonant mode calculates a density almost two orders of magnitude less than the

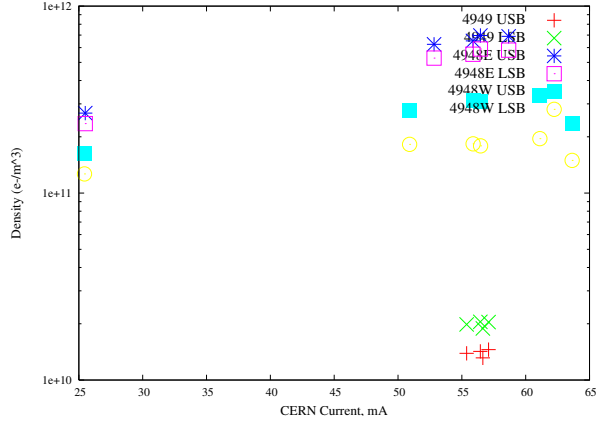


Figure 18: The following depicts the calculated ECD by the various means in the L3 region, with the Chicane off on a log y scale, 4ns spacing.

transmission method, which is why the data was plotted on a log y scale. No meaningful relation can currently be determined from the effect of the Chicane field (data not shown).

VI. DISCUSSION

We have applied the use of microwave dispersion techniques to measuring the ECD in CESR. In addition, we have developed a novel technique to measure local densities by use of an resonant mode. Both methods agree to first order with ECD found elsewhere, and are qualitatively similar to raw RFA current data. A more detailed analysis with densities from RFA simulations will help elucidate the characteristics of the data shown here.

The ECD found in the rectangular beam pipe in the L0 region is in better agreement

than density data from the L3 region, where circular pipe is used. This may indicate that the fields in the circular pipe do not sample the same regions of the beam pipe. However, densities typically do not vary by two orders of magnitude over the beam pipe.

Transmission, resonant and RFA data agree to first order. However, the transmission measurements are clearly higher than other measurements, which could be caused by reflections. At least part of the asymmetry between upper and lower sidebands is certainly caused by the transfer function of the beam pipe, which we have shown needs to be measured near the time of the measurement. It might be possible to use a signal from power supply noise, or amplitude modulate the carrier to get additional sidebands which could be used for calibration. Other factors could include amplitude and phase modulation.

The resonant mode developed here allowed for local measurements without unnecessary complexity. Furthermore, the resonant mode is much more sensitive than the transmission method. The calculation for the dispersion relation needed in the transmission method for a non-uniform plasma is formidable, while we have shown that for the resonant method, the calculation is relatively straight forward, and can often be done analytically. While it is often not necessarily to

include a specific distribution of ECD, it allows for the possibility of accounting for non-uniformity, should the distribution become important.

The CESR beam pipe has many discontinuities, thus concern has been raised regarding reflections of a propagating wave. Since the resonant mode allows for a local measurement, this is no longer a concern. However, the resonant method does bring up additional questions. For instance, the energy stored in the cavity has a finite Q , and if the time constant of the cavity approaches the decay time of the EC, the effect could become important.

A sinusoidal oscillation of the EC has been assumed, which yields a time averaged density. However, the first term of the Fourier series for a square pulse allows the peak density to be calculated to first order. This method, while accurate does not account for the decay time of the EC. This question would be elucidated by measurements of the EC in the time domain. Such a measurement could be performed by measuring the phase shift of frequency shift as a function of time on an oscilloscope.

VII. ACKNOWLEDGMENTS

Special thanks also goes to my mentors, Mike Billing, Mark Palmer, and John Sikora who taught me a great deal of physics

and worked closely with me on this project. Thanks also to Joe Calvey and Jessey Livezy for help with RFA data, Stefano De Santis for many helpful conversations, and to Becky Kraft for proof reading. This work was supported by the National Science Foundation REU grant PHY-0849885.

-
- [1] Z. Ya-Jin, M. Wen-Gan, H. Liang, and Z. Ren-You, *Phys. Rev. D* **76**, 054003 (2007).
- [2] H.K. Dreiner, O. Kittel, and U. Langenfeld, *Phys. Rev. D* **74**, 115010 (2006).
- [3] T. Moroi and Y. Shimizu, *Phys. Rev. D* **72**, 115012 (2005).
- [4] M.A. Furman, *New Journal of Physics*, **8**, 289 (2006).
- [5] Alexei V. Smirnov, *Review of Scientific Instruments*, **80**, 013301 (2009).
- [6] R. Cimino, I. R. Collins, M. A. Furman, M. Pivi, F. Ruggiero, G. Rumolo, and F. Zimmermann, *Phys. Rev. Lett.* **93**, 014801.
- [7] M. Izawa, Y. Sato, and T. Toyomasu, *Phys. Rev. Lett.* **74**, 5044 (1995).
- [8] G. Rumolo, A. Z. Ghalam, T. Katsouleas, C. K. Huang, V. K. Decyk, C. Ren, W. B. Mori, F. Zimmermann, and F. Ruggiero, *Phys. Rev. ST. Accel. and Beams* **6**, 081002 (2003).
- [9] K. Ohmi and F. Zimmerman, *Phys. Rev. Lett.* **85**, 3821 (2000).
- [10] F. Zimmermann, *Phys. Rev. ST. Accel. and Beams* **7**, 124801 (2004).
- [11] K.C. Harkay, R.A. Rosenberg, *Phys. Rev. ST. Accel. and Beams* **6**, 034402 (2003).
- [12] M.A. Furman, M.T.F. Pivi, *Phys. Rev. ST. Accel. and Beams* **5**, 124404 (2002).
- [13] Y.Suetsugu, H.Fukuma, L.Wang, M.Pivi, A.Morishige, Y.Suzuki, M.Tsukamoto, M.Tsuchiya, *Nucl. Instrum. Methods Phys. Res., Sect. A* **598**, 372 (2009).
- [14] Y.Suetsugu, H.Fukuma, M.Pivi b, L.Wang, *Nucl. Instrum. Methods Phys. Res., Sect. A* **604**, 449 (2009).
- [15] F-J. Decker, R.L. Holtzapple, A. Kulikov, M. Sullivan, in: *Proceedings of the 2002 European Particle Accelerator Conference, Paris, 3-7 June, 2002*, pp. 392-394.
- [16] R.A. Rosenberg, and K.C. Harkay, *Nucl. Instrum. Methods Phys. Res., Sect. A* **453**, 507 (2000).
- [17] S. De Santis, J.M. Byrd, F. Caspers, A. Krasnykh, T. Kroyer, M.T.F. Pivi, and K.G. Sonad, *Phys. Rev. Lett.* **100**, 094801 (2008).
- [18] L. Tonks and I. Langmuir, *Phys. Rev.* **33**, 195 (1929).
- [19] G.I. Zaginaylov, *Phys. Rev. E.* **64**, 016406 (2001).

- [20] A.W. Trivelpiece and R.W. Gould, *J. Appl. Phys.* **30**, 1784 (1959).
- [21] H.S. Uhm, K.T. Nguyen, R.F. Schneider, and J.R. Smith, *J. Appl. Phys.* **64**, 1108 (1988).
- [22] K. Sonnad, M. Furman, S. Veitzer, P. Stoltz, and J. Cary, in *Proceedings of the 2007 Particle Accelerator Conference, Albuquerque, New Mexico*, 2007 (IEEE, Piscataway, NJ, 2007).
- [23] H. S. Black, *Modulation Theory* (D. Van Nostrand Co., Princeton NJ, 1953).
- [24] M.A. Heald, C.B. Wharton, *Plasma Diagnostics With Microwaves* (John Wiley and Sons Inc., New York, 1965).
- [25] S. Ramo, J.R. Whinnery, T. van Duzer, *Fields and Waves in Communication Electronics* (John Wiley and Sons Inc., New York, 1965).
- [26] R.E. Collin, *Foundations for Microwave Engineering, Second Edition* (IEEE Press, New York, 2001).
- [27] Y.S. Yeh and W.A. Saxton, *Modified Theory for Cavity Perturbation Measurement of Plasma Parameters*, Scientific Report No. 5, NASA (1969).
- [28] S.J. Buchsbaum and S. C. Brown, *Phys. Rev.* **106**, 196 (1957).
- [29] K.B. Persson, *Phys. Rev.* **106**, 191 (1957).
- [30] M.A. Palmer, M. Billing, J. Calvey, G. Codner, S. Greenwald, Y. Li, X. Liu, J. Livezey, R. Meller, R. Schwartz, J. Sikora, C. Strohman, W. Whitney, T. Wilksen, in *Proceedings of the 2009 Particle Accelerator Conference, Vancouver*, TH5RFP030, 2009.
- [31] J. Calvey, J.A. Crittenden, G. Dugan, S. Greenwald, D. Kreinick, J.A. Livezey, M.A. Palmer, D. Rubin, K.C. Harkay, P. Jain, K. Kanazawa, Y. Suetsugu, C.M. Celata, M. Furman, G. Penn, M. Venturini, M.T.F. Pivi, L. Wang, in *Proceedings of the 2009 Particle Accelerator Conference, Vancouver*, FR5RFP043, 2009.